NJC

LETTER

View Article Online
View Journal | View Issue



Cite this: *New J. Chem.*, 2015, 39, 2400

Received (in Montpellier, France) 31st October 2014, Accepted 15th January 2015

DOI: 10.1039/c4nj01933d

www.rsc.org/njc



# Separation of $CO_2$ from $CH_4$ and $CO_2$ capture in the presence of water vapour in NOTT-400†

Maximiliano R. Gonzalez,[a] Juan H. González-Estefan,[b] Hugo A. Lara-García,[b] Pedro Sánchez-Camacho,[b] Elena I. Basaldella,[ac] Heriberto Pfeiffer[b] and Ilich A. Ibarra*[b]

**From a binary equimolar gas-mixture of $CO_2$ and $CH_4$, NOTT-400 shows $CO_2$ separation from $CH_4$. By kinetic uptake experiments, this material confirms a maximum of 4.3 wt% $CO_2$ capture at 30 °C and a significant 2-fold increase (~9.3 wt%) in $CO_2$ capture under 40% relative humidity of water vapour.**

Air pollution and global warming are two of the foremost threats to our civilisation.[1–6] Of particular significance are the rapidly increasing levels of carbon dioxide ($CO_2$) emissions, due to burning of fossil fuels. Fossil fuels are non-renewable[7] and cannot continue as a principal energy source in the far future[8] due to the limited reserves. Natural gas ($CH_4$) is a very desirable fuel because it burns cleaner than any other fossil fuel (*e.g.* petrol or coal).[9] However, the quality of natural gas, coming from land fields and biogas plants, is considerably low with impurities like $CO_2$ (20 to 35%), $N_2$, $H_2O$ and $H_2S$.[10] Then, pre-combustion $CO_2$ capture from natural gas is essential to maximise its energy content. Additionally, post-combustion $CO_2$ capture from plant flue gas is also crucial in order to control greenhouse emissions.[11]

$CO_2$ separation and sequestration have extremely motivated many governments to invest in the development of new methods for efficiently and effectively capturing $CO_2$.[12] Conventional adsorption in aqueous alkanolamine solutions has been extensively used and studied, but they have many major limitations as adsorbents for industrial $CO_2$ capture due to their heat instability and corrosion towards vessels and pipelines.[13] Thus, the use of porous solids for the adsorption of $CO_2$ is a timely research area and the search for materials with a high adsorption capacity, structural stability, fast sorption kinetics and mild regeneration properties remains a major challenge.

Porous coordination polymers (PCPs) or metal–organic frameworks (MOFs) are amongst the most promising candidates for gas separation, because their sorption selectivity towards small molecule adsorbates is directly tunable as a function of the topology and chemical composition of the micropores.[14,15] Despite the high $CO_2$ capacity and selectivity that PCPs show, many gas separation processes involve the exposure to water vapour. However, few PCPs have shown good stability to water, and water is most often unfavourable to gas separations.[16] Among those few examples, Hong *et al.*[17] reported a water-stable PCP based on a binuclear [$In_2(\mu_2$-OH)] building block (see Scheme S1, ESI†), InOF-1, constructed from a flexible $BPTC^{4-}$ ligand ($H_4BPTC$ = biphenyl-3,3′,5,5′-tetracarboxylic acid) which also showed high $CO_2/N_2$ and $CO_2/CH_4$ selectivities (by using the experimental single-component gas adsorption isotherms). Interestingly, the effect of water on the $CO_2$ capture has only recently been investigated on PCPs.[18,19]

Llewellyn and co-workers[20] investigated the $CO_2$ adsorption in some PCPs under different relative humidities of water vapour. Indeed, HKUST-1 was shown to degrade in the presence of humidity, and UiO-66 did not show any enhanced $CO_2$ uptake.[20] In the case of MIL-100(Fe), a remarkable 5-fold increase in $CO_2$ uptake was observed with increasing relative humidity (RH), 105 mg $g^{-1}$ at 40% RH. Additionally, Yaghi *et al.*[21] showed that the presence of hydroxyl functional groups increases the affinity of the framework for water. Thus, in the present work we have chosen a material entitled NOTT-400[22] based on a binuclear [$Sc_2(\mu_2$-OH)] building block (see Scheme S1, ESI†) which is isostructural to the water-stable InOF-1[17] and possesses hydroxo functional groups ($\mu_2$-OH) to study the separation of a binary gas mixture (not a single-component gas) of $CO_2$ and $CH_4$ and we have successfully performed $CO_2$ capture in the presence of water vapour.

After the first gas separation experiment was carried out (see Experimental), the most characteristic FTIR bands for the $CO_2$ (2349 $cm^{-1}$) and $CH_4$ (3016 $cm^{-1}$) molecules were analysed. In Fig. 1 it is possible to observe a continuous increase in the

[a] *Centro de Investigación y Desarrollo en Ciencias Aplicadas Dr. J. J. Ronco (CINDECA), (CONICET-CIC-UNLP) 47 No. 257, (B1900 AJK) La Plata, Argentina*
[b] *Instituto de Investigaciones en Materiales, Universidad Nacional Autónoma de México, Circuito Exterior s/n, CU, Del. Coyoacán, 04510, Mèxico D. F., Mexico. E-mail: argel@unam.mx*
[c] *CITEMA, Universidad Tecnológica Nacional, 60 y 124, (1900) La Plata, Argentina*

† Electronic supplementary information (ESI) available: TGA data, PXRDP data, FTIR data, polynomial regressions and kinetic uptake experiments. See DOI: 10.1039/c4nj01933d

 

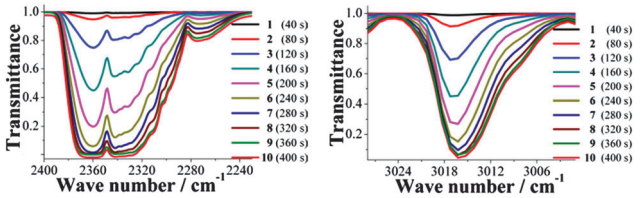


Fig. 1 FTIR spectra of the resulting exit exhaust of the binary equimolar (0.13 mmol $min^{-1}$) gas-mixture of $CO_2$ and $CH_4$: (left) the characteristic $CO_2$ band and (right) the characteristic $CH_4$ band.

characteristic band intensities (Fig. 1) for $CO_2$ and $CH_4$ with time. In other words, from spectrum 1 to spectrum 10 the intensity of the characteristic FTIR band increases while the transmittance decreases.

The intensities of these characteristic FTIR bands (for $CO_2$ and $CH_4$) were shown to be different. This could suggest that the $CO_2$ and $CH_4$ molecules arrive at the FTIR detector with different times. By normalising the intensities, considering their respective transmittances, it is possible to plot the increase in intensity of each scan for $CO_2$ and $CH_4$ simultaneously (Fig. 2, left). For each scan, the normalised intensity of $CH_4$ is higher than $CO_2$, suggesting that the molecules of $CH_4$ effectively arrive at the FTIR detector before the $CO_2$ molecules. We can rationalise this result as follows: when the binary gas mixture ($CO_2$ and $CH_4$) flows through the activated sample NOTT-400 this material retains $CO_2$ stronger than $CH_4$, and therefore, the $CH_4$ gas molecules flow 'faster' inside the material and are detected earlier. In order to confirm this hypothesis, we carried out three more experiments: first, an acetone-exchanged sample of NOTT-400 (40 mg) was placed into the BEL-REA system, activated and stabilised as described (*vide supra*) and a flow of only $CO_2$ gas (0.13 mmol $min^{-1}$) was set. Then, the resulting flow gas was analysed by FTIR spectroscopy and 10 scans were recorded, until the detector was saturated (see Fig. S5, ESI†). Second, another acetone-exchanged NOTT-400 (40 mg) sample was mounted in the BEL–REA system, activated, stabilised and analysed as described earlier. This time, the sample was exposed to a flow of only $CH_4$ gas (0.13 mmol $min^{-1}$). As in the previous experiment, 10 FTIR spectra were collected from the resulting flow gas until the detector was saturated (see Fig. S6, ESI†). Again, by normalising the characteristic FTIR intensities it was possible to simultaneously plot the normalised intensity of each scan for $CO_2$ and $CH_4$ (Fig. 2, right).

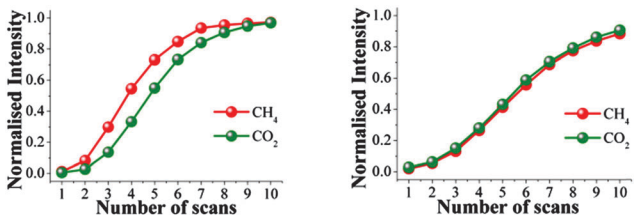


Fig. 2 Normalised characteristic FTIR intensities of $CO_2$ and $CH_4$ as a function of the number of scans. (left) FTIR intensities from a resulting exit exhaust of the binary equimolar (0.13 mmol $min^{-1}$) gas-mixture of $CO_2$ and $CH_4$; (right) FTIR intensities from individual flows of $CO_2$ and $CH_4$.

Thus, the normalised intensities for $CO_2$ and $CH_4$ at each scan (from 1 to 10) are practically the same (Fig. 2, right) suggesting that when the resulting flow of each pure-gas component (not a mixture of gases) is analysed separately by FTIR spectroscopy, the molecules of $CO_2$ and $CH_4$ arrive at the same time to the FTIR detector. These results confirm that NOTT-400 is more selective to $CO_2$ than $CH_4$ when a binary equimolar (0.13 mmol $min^{-1}$) gas-mixture of $CO_2$ and $CH_4$ flows though an activated sample. We interpreted this selectivity as the time delay of the $CO_2$ molecules in reaching the FTIR detector. By polynomial regressions of the normalised intensities in Fig. 2 (left), we estimated this delay to be ~28 s (see Fig. S7 and S8, ESI†). Finally a third experiment was carried out: in order to confirm that this delay was caused by the adsorption selectivity shown by NOTT-400 (a microporous PCP) rather than other phenomena, a non-porous material was mounted in the BEL–REA system. PCM-14[23] is a dense coordination polymer that has shown to be a non-porous material when it is activated between 25–150 °C. Thus, a sample of PCM-14 (40 mg) was activated at 150 °C for 2 h under a flow of $N_2$ gas and then directly exposed to a binary equimolar (0.13 mmol $min^{-1}$) $CO_2$ and $CH_4$ gas mixture. Thus, the resulting flow gas was analysed by FTIR spectroscopy and just 6 scans were recorded, until the detector was saturated. By normalisation of the characteristic FTIR intensities, we plotted the normalised intensities of each $CO_2$ and $CH_4$ scan (see Fig. S9, ESI†). Interestingly, the normalised intensities for $CO_2$ and $CH_4$ at each scan (from 1 to 6) are practically the same (see Fig. S9, ESI†) confirming that the time delay is due to the microporosity of NOTT-400.

Dynamic and isothermal $CO_2$ experiments were carried out on NOTT-400 (see Experimental thermobalance, ESI†). Fig. 3, left, shows the kinetic uptake experiments from 30 °C to 100 °C. At 30 °C the material exhibited the maximum weight% gain, which represents the maximum amount of $CO_2$ captured.

This amount corresponds to 4.3 wt% and it was rapidly reached after just ~300 s (5 min) and it remained constant until the end of the experiment (3600 s or 60 min). At 40 °C the uptake was estimated to be 3.5 wt% and it was also reached after around 300 s (Fig. 3, left). Clearly, while the temperature is increased (from 30 to 100 °C), the $CO_2$ weight(%) decreases gradually (Fig. 3, left) to 0.5 wt% (at 100 °C). In order to confirm that this decrease is not due to sample degradation, we have run PXRD measurements on each sample after these $CO_2$ capture experiments. Fig. 3 (right)

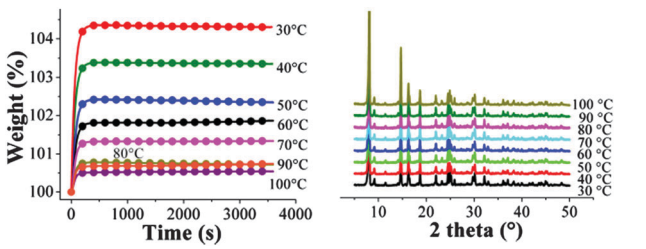


Fig. 3 (left) Kinetic uptake experiments performed at different temperatures (30, 40, 50, 60, 70, 80, 90 and 100 °C) with a $CO_2$ flow of 60 mL $min^{-1}$. Each curve shows the experimental data and the symbols were used to differentiate them; (right) PXRD patterns of each NOTT-400 sample after the kinetic $CO_2$ isotherms were carried out at different temperatures.

shows that the crystallinity of the samples after each $CO_2$ capture experiment was retained. Indeed, we increased the temperature progressively up to 650 °C (see Fig. S10, ESI†) and there is a constant weight loss, suggesting that samples of activated NOTT-400 are not capturing $CO_2$ after 150 °C and what we observe is a gradual structural decomposition which was confirmed by PXRD (see Fig. S10, ESI†).

Motivated by the very promising results that Hong *et al.* reported,[17] by showing an isostructural framework to NOTT-400 (InOF-1), which is water stable and exhibited high $CO_2/N_2$ and $CO_2/CH_4$ selectivities, we explored the water stability of NOTT-400. Then, acetone-exchanged samples of NOTT-400 were exposed to air and soaked in distilled water. PXRD patterns of these experiments (see Fig. S11, ESI†) then confirmed the structural stability of NOTT-400 in water. This water-stability can be attributed to the presence of the hydroxo functional groups (within the pores of NOTT-400) which has been previously shown[21] and these functional groups enhance the affinity of the material for water. Thus, after establishing the best $CO_2$ capture temperature (30 °C, Fig. 3, left), a kinetic isotherm experiment at 30 °C, with a constant $CO_2$ flow and a relative humidity (RH) of 40%, was carried out. It was decided to run this experiment with a 40% RH based on the remarkable results that Llewellyn *et al.*[20] previously reported (5-fold increase in $CO_2$ uptake for MIL-100(Fe)).

An activated NOTT-400 sample (150 °C for 2 h and under a flow of $N_2$ gas) was placed into a humidity-controlled thermobalance. After activation of the material, the equipment was stabilised at 40% RH (30 °C) and a constant $CO_2$ flow (60 mL $min^{-1}$) was started. Later, we repeated this experimental procedure on a different activated NOTT-400 sample and set a constant $N_2$ flow (60 mL $min^{-1}$). Fig. 4 shows the kinetic uptake experiments at 30 °C and 40% RH for $CO_2$ and $N_2$. For both isotherms, it is clearly observed that the material shows a constant increase in weight (while the experiment is progressing with time, see Fig. 4). This increase in weight is due the contribution of water and $CO_2$ or water and $N_2$, respectively.

In order to find the maximum $CO_2$ capture under 40% RH conditions, we need to differentiate the contribution of water to the weight increase. By simply taking the difference of the two isotherms ($CO_2$ and $N_2$) we could obtain the $CO_2$ captue at 40% RH. This is valid if the material does not capture any $N_2$ at 30 °C. Therefore, by performing a kinetic uptake experiment on an activated NOTT-400 sample at 30 °C without any presence of water vapour (0% RH) with a constant $N_2$ flow (60 mL $min^{-1}$) we obtained a $N_2$ capture of approximately 0.01 wt%. This result is consistent with previous reports where the capacity of $N_2$ capture in PCPs at room temperatures is basically negligible.[24] In Fig. 4, the gradual weight increase (for $CO_2/H_2O$ and $N_2/H_2O$) starts at 0 s and stabilises at ~6000 s (100 min). Interestingly, under anhydrous conditions the $CO_2$ uptake rapidly reached stability (5 min, see Fig. 3, left). This equilibrium discrepancy is due to the nature of the vapour adsorption process that in general takes considerably more time to reach stability than the gas adsorption process in microporous materials.[25] Then, from 600 s until approximately 11 000 s (183.3 min) both isotherms seem to reach a plateau where both uptakes are practically constant. At 11 000 s, the maximum amounts of $CO_2/H_2O$ and $N_2/H_2O$ captured are 51.1 wt% and 41.8 wt%, respectively and by taking the difference of these two values (since there is no $N_2$ uptake at 30 °C) the $CO_2$ capture in the materials is ~ 9.3 wt%. Finally, from 11 000 s to 13 000 s (Fig. 4, red rectangle) the flow of each gas and the relative humidity were stopped and the decrease in weight represents the gas and water vapour desorption. Therefore, the $CO_2$ capture was approximately 2-fold increased with a 40% RH. This enhancement in $CO_2$ uptake in the presence of water can be explained by $CO_2$ confinement effects induced by bulky molecules ($H_2O$).[26] Additionally, we decided to run a $CO_2$ experiment (60 mL $min^{-1}$) at 40% RH and 30 °C on an activated PCM-14[23] sample (150 °C for 2 h, under a flow of $N_2$ gas). Since PCM-14 is a non-porous material, when activated between 25–150 °C, it provided a direct $CO_2$ capture comparison to NOTT-400 (microporous material). Thus, from 0 s to 11 000 s the maximum $CO_2$ uptake (under 40% RH) was 0.8 wt% (see Fig. S12, ESI†). This result corroborated that there is no $CO_2$ sequestration in a non-porous material when the relative humidity is 40% at 30 °C.

In summary, the Sc(III) coordination polymer NOTT-400 shows $CO_2$ separation from $CH_4$, in a more realistic scenario, when this material was exposed to a binary, $CO_2/CH_4$, equimolar gas-mixture. By kinetic isotherm experiments, NOTT-400 exhibits a total $CO_2$ amount of 4.3 wt% at 30 °C, which was rapidly reached after just approximately 300 s. Additionally, NOTT-400 exhibits high stability towards humidity, which was confirmed by PXRD. Due to this particularly high stability, NOTT-400 performs $CO_2$ uptake under relative humidity conditions (40% RH) and 30 °C, displaying a maximum $CO_2$ capture of approximately 9.3 wt%.

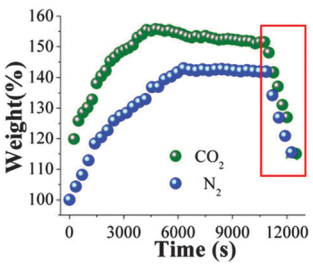


Fig. 4 Kinetic uptake experiments carried out at 30 °C and 40% RH with $CO_2$ (green spheres) and $N_2$ (blue spheres) flows of 60 mL $min^{-1}$, respectively.

## Experimental

### Gas separation experiments

A catalytic reactor system (BEL-REA, BEL Japan; Fig. S3, ESI†) was employed, which allowed each sample of acetone-exchanged NOTT-400 (see Experimental, ESI†) to be activated (150 °C for 2 h) under a flow of $N_2$ gas and then directly exposed to adsorbates ($CO_2$ and $CH_4$) *in situ*, and studied by FTIR spectroscopy over many cycles without physical manipulation or exposure to air. In each study, an acetone-exchanged sample of NOTT-400 (40 mg) was placed into the holder sample in the BEL–REA system and activated as described above. Then, the system was allowed to cool down to 30 °C and the activated sample was exposed to a

 

flow of the binary equimolar (0.13 mmol $min^{-1}$) gas mixture of $CO_2$ and $CH_4$. This mixture represents a more realistic composition for gas separation processes. Next, after stabilisation of the gas flow within the sample, the resulting exit exhaust gases (see Fig. S3, ESI†) was analysed by FTIR spectroscopy. Thus, each FTIR spectrum was recorded every 40 seconds ($\sim$0.66 min), until the detector was saturated, to make a total of 10 FTIR spectra (see Fig. S4, ESI†).

## Acknowledgements

The authors thank Dr A. Tejeda-Cruz (X-ray; IIM-UNAM) and CONACyT Mexico (212318) for financial support. M.R.G. thanks CONICET and BECAR Argentina for scholarship funding. Thanks to U. Winnberg for scientific discussions.

## Notes and references

1 F. W. Lipfert, *Air Pollution and Community Healt: A Critical Review and Data Source Book*, Van Nostrand Reinhold, New York, USA, 1994, p. 556.
2 P. D. Noyes, M. K. McElwee, H. D. Miller, B. W. Clark, L. A. Van Tiem, K. C. Walcott, K. N. Erwin and E. D. Levin, *Environ. Int.*, 2010, **35**, 971.
3 J. F. Zhang and K. R. Smith, *Br. Med. Bull.*, 2003, **68**, 209.
4 J. T. Litynski, S. M. Klara, H. G. McIlvried and R. D. Srivastava, *Environ. Int.*, 2006, **32**, 128.
5 M. Z. Jacobson, *Energy Environ. Sci.*, 2009, **2**, 148.
6 International Energy Agency (IEA), Key World Energy Statistics, OECD/IEA, France, 2013.
7 M. Z. Jacobson, *Geochim. Cosmochim. Acta*, 2009, **73**, A581.
8 A. Züttel, A. Borgschulte and L. Schlapbach, *Hydrogen as a Future Energy Carrier*, Wiley-VCH, Weinheim, Germany, 2008, p. 441.
9 T. Burchell and M. Rogers, *SAE Tech. Pap. Ser.*, 2000, 2000.
10 M. Herout, J. Malat'ák, L. Kučera and T. Dlabaja, *Res. Agric. Eng.*, 2011, **57**, 137.
11 D. M. D'Alessandro, B. Smit and J. R. Long, *Angew. Chem., Int. Ed.*, 2010, **49**, 6058.
12 K. Sumida, D. L. Rogow, J. A. Mason, T. M. McDonald, E. D. Bloch, Z. R. Herm, Z. T.-H. Bae and J. R. Long, *Chem. Rev.*, 2012, **112**, 724.
13 (*a*) G. T. Rochelle, *Science*, 2009, **325**, 1652; (*b*) F. Karadas, M. Atilhan and S. Aparicio, *Energy Fuels*, 2010, **24**, 5817.
14 (*a*) S. Yang, G. S. B. Martin, G. J. J. Titman, A. J. Blake, D. R. Allan, N. R. Champness and M. Schröder, *Inorg. Chem.*, 2011, **50**, 9374; (*b*) A. J. Nuñez, L. N. Shear, N. Dahal, I. A. Ibarra, J. W. Yoon, Y. K. Hwang, J.-S. Chang and S. M. Humphrey, *Chem. Commun.*, 2011, **47**, 11855.
15 (*a*) H. Furukawa, N. Ko, Y. B. Go, N. Aratani, S. B. Choi, E. Choi, A. Ö. Yazaydin, R. Q. Snurr, M. O'Keeffe, J. Kim and O. M. Yaghi, *Science*, 2010, **329**, 424; (*b*) A. M. Bohnsack, I. A. Ibarra, P. W. Hatfield, J. W. Yoon, Y. K. Hwang, J.-S. Chang and S. M Humphrey, *Chem. Commun.*, 2011, **47**, 4899; (*c*) P. Nugent, Y. Belmabkhout, S. D. Burd, A. J. Cairns, R. Luebke, K. Forrest, T. Pham, S. Ma, B. Space, L. Wojtas, M. Eddaoudi and M. J. Zaworotko, *Nature*, 2013, **495**, 80.
16 (*a*) S. S. Nagarkar, A. K. Chaudhari and S. K. Ghosh, *Inorg. Chem.*, 2012, **51**, 572; (*b*) H. J. Choi, M. Dincă, A. Daily and J. R. Long, *Energy Environ. Sci.*, 2010, **3**, 117.
17 J. Qian, F. Jiang, D. Yuan, M. Wu, S. Zhang, L. Zhang and M. Hong, *Chem. Commun.*, 2012, **48**, 9696.
18 (*a*) J. Liu, A. I. Benin, A. M. B. Furtado, P. Jakubczak, R. R. Willis and M. D. LeVan, *Langmuir*, 2011, **27**, 11451; (*b*) A. C. Kizzie, A. G. Wong-Foy and A. J. Matzger, *Langmuir*, 2011, **27**, 6368; (*c*) H. Jasuja, Y.-g. Huang and K. S. Walton, *Langmuir*, 2012, **28**, 16874; (*d*) H. Jasuja, J. Zang, D. S. Sholl and K. S. Walton, *J. Phys. Chem. C*, 2012, **116**, 23526; (*e*) J. B. DeCoste, G. W. Peterson, H. Jasuja, T. G. Glover, Y.-g. Huang and K. S. Walton, *J. Mater. Chem. A*, 2013, **1**, 5642.
19 J. Liu, Y. Wang, A. I. Benin, P. Jakubczak, R. R. Willis and M. D. LeVan, *Langmuir*, 2010, **26**, 14301.
20 E. Soubeyrand-Lenoir, C. Vagner, J. W. Yoon, P. Bazin, F. Ragon, Y. K. Hwang, C. Serre, J.-S. Chang and P. L. Llewellyn, *J. Am. Chem. Soc.*, 2012, **134**, 10174.
21 H. Furukawa, F. Gándara, Y.-B. Zhang, J. Jiang, W. L. Queen, M. R. Hudson and O. M. Yahgi, *J. Am. Chem. Soc.*, 2014, **136**, 4369.
22 I. A. Ibarra, S. Yang, X. Lin, A. J. Blake, P. J. Rizkallan, H. Nowell, D. R. Allan, N. R. Champness, P. Hubberstey and M. Schröder, *Chem. Commun.*, 2011, **47**, 8304.
23 I. A. Ibarra, K. E. Tan, V. M. Lynch and S. M. Humphrey, *Dalton Trans.*, 2012, **41**, 3920.
24 (*a*) E. Haldoupis, S. Nair and D. S. Sholl, *J. Am. Chem. Soc.*, 2012, **134**, 4313; (*b*) Y.-S. Bae, O. K. Farha, J. T. Hupp and R. Q. Snurr, *J. Mater. Chem.*, 2009, **19**, 2131.
25 I. P. O'koye, M. Benham and K. M. Thomas, *Langmuir*, 1997, **13**, 4054.
26 N. L. Ho, F. Porcheron and R. J.-M. Pellenq, *Langmuir*, 2010, **26**, 13287.